Quest Journals
Journal of Research in Mechanical Engineering
Volume 8 ~ Issue 5 (2022) pp: 39-49
ISSN(Online) : 2321-8185
www.questjournals.org

Research Paper

Fabrication of a Multi-Lumen Diameter Common Carotid Artery Wall-Less Phantom for Doppler Ultrasound Studies

Pam S.D [1]*(FWACS), Dakok K.K[2] (PhD) Sirisena A U.I[1](PhD), Nabasu S.E [2] (MSc)

1. Jos University Teaching Hospital Jos, Plateau State, Nigeria.
2. Department of Physics, Plateau State University Bokkos, P.O Box 2012, Plateau Sate, Nigeria
Corresponding Author: dakokkyense@gmail.com

Abstract
Flow phantoms with anatomically realistic geometry and high acoustic compatibility with real vessels are reliable tools in vascular ultrasound studies. We present a multi-lumen diameter common carotid artery (CCA) wall-less phantom for ultrasound studies of relationship between lumen diameter and flow velocity. The phantom was constructed with 8 lumen diameters from 4.5 mm to 8.0 mm with an acoustic depth of 7.5 mm all within normal human carotid geometry. The tissue mimicking material (TMM) consists of konjac, carrageenan and gelatin as basic components mixed with other suitable components. The blood-mimicking fluid (BMF) was prepared by mixing propylene glycol, Glucose and poly 4-methystyrene scatterers in distilled water. The constructed phantom was scanned using ultrasound machine to measure flow velocities through the lumens and to test the quality of the phantom. The phantom was found to be robust and strong with a speed of sound and attenuation of 1548±0.07 m/s while the attenuation was 0.5±0.02 dB/cm at 5 MHz frequency. An inverse relationship was established between the CCA diameter with the peak systolic velocity (PSV), end diastolic velocity (EDV) and average velocity of the BMF. The relationship between carotid diameter and flow velocities can be used to estimate the degree of stenosis in the CCA for much narrowed vessels.

Keywords: *Tissue Mimicking Material; Blood Mimicking Fluid; Common Carotid artery; Flow Velocity; Doppler Ultrasound; Wall-less Phantom.*

***R**eceived 16 May, 2022; **R**evised 28 May, 2022; **A**ccepted 30 May, 2022 © The author(s) 2022.*
P**ublished with open access at **www.questjournals.org

I. Introduction

Training of Sonographers and researches in ultrasound imaging can be essentially carried out with phantoms as clinical tools. They are useful for the development of Doppler ultrasound (DU) techniques for investigating blood flow. These phantoms mimic flow characteristics within blood vessels both for clinical ultrasound studies whose frequencies are from 2MHz to 15MHz and for preclinical ultrasound where higher frequencies between15MHz to 60MHz are used [1, 2, 3,4]. For compatibility between ultrasound images of phantoms and those from human or animal body, it is important to make sure that the relevant physical and acoustic properties of these flow phantoms match the properties of human/animal tissues [5]. Flow phantoms for DU studies are made up of Tissue Mimicking materials (TMM) to match the acoustic properties of soft tissues, a blood mimicking fluid (BMF) to match the acoustic properties of viscous blood, and a Vessel Mimicking material (VMM) to match the acoustic properties of the vessel wall. A pump is always required to circulate the BMF in a flow loop. For wall-less phantoms, the TMM is in direct contact with the BMF [6]. It has the advantage of avoiding mismatch problems in acoustic properties [7, 8] over walled phantoms. However, its properties may be affected when the TMM is exposed to air or water [9].

Assessment of the severity of plaques is primarily centered on the values of peak systolic velocity (PSV) and narrowing of the lumen mostly in the internal carotid artery (ICA). This leaves the common carotid artery (CCA) PSV with more research to find out how it can be useful in categorizing percentage stenosis [10, 11, 12]. In vitro researches using carotid artery phantoms for studying the degree of stenosis have also put their concentration on the use of PSV in the ICA as one of their primary considerations for plaque assessment [13, 14,

15, 16, 17, 18, 19, 20]. Therefore, there is a need for a single wall-less flow phantom with several lumen diameters to establish a relationship between CCA diameter and flow velocity. It is in this light that we have constructed a wall-less CCA phantom with 8 different lumen diameters representing the normal range for 8 healthy arteries from 4.5 mm to 8.0 mm. A relationship between the carotid diameter with flow velocity using this phantom helps in estimating the values of the PSV, end diastolic velocity (EDV) and average velocity of narrowed lumens of even 1.0 mm or large lumen of up to 10.0 mm or more. The diameters of a healthy human CCA, ICA and external carotid artery (ECA) are 6.0 mm, 4.2 mm and 3.5 mm respectively with a normal range of 4.3 mm – 7.7 mm for the CCA, but women have higher artery diameters compared to men [21, 22, 6, 23, 24].

II. Materials and Methods

The procedures for the construction of this phantom spans from the design and construction of the phantom box, preparing the TMM, casting of the TMM in the phantom box, BMF preparation, testing of the phantom using a gear pump to pump the BMF and a DU machine to measure the flow velocities.

2.1 Construction of the Phantom Box

The phantom box was designed with rectangular dimensions of 45 cm x 25 cm x 9 cm and made of transparent plexiglass (acrylic) material covered at the bottom and opened at the top. Eight different holes were bored exactly at heights of 5 cm on each side of the box length directly opposite each other to house 8 different straight metallic rods of diameters 4.5 mm, 5.0 mm, 5.5 mm, 6.0 mm, 6.5 mm, 7.0 mm, 7.5 mm and 8.0 mm to represent the lumen diameters of the common carotid arteries. The stainless steel rods were machined by a company (PLC Solutions, 34200 Parit Buntar Perak, Malaysia, using CNC lathe machine) into the required diameters to ensure that they fit horizontally into the holes**.** Reticulated foam with a pore size of 1–2 mm was glued with Araldite to the inside wall and around the pipe connectors in the box. This was done to provide a fixed structure into which the TMM can set properly to prevent it from contracting away from the connectors and to ensure that the BMF does not leak during the flow. The rods were inserted through both of the opposite pipe connectors, which were aligned to make sure that they were straight (figure 1a).

2.2 Preparation and casting of the TMM

The TMM adopted for the wall-less phantom in this research is the Konjac-Carrageenan (KC) and gelatin based mimicking material [25] because it has the advantage of not being ruptured during fast flow unlike the KC-based wall-less phantoms that suffers from rupturing [5]. The TMM constituents, percentage weight/weight (% w/w), manufactories and their uses are summarized in table 1.

Table 1: Constituents of Konjac-Carrageenan and gelatin based tissue mimicking material (TMM) for wall-les phantom

Name of substance	Percentage Composition (% w/w)	Manufacturer	Function
Distilled water	84.0	-	Serves as a solvent
Silicon Carbide (400 grain size)	0.53	Logitec, Glasgow, UK	Serves as scatterers
Al_2O_3 powder (3 μm)	0.96	Sigma-Aldrich, Germany	Serves as scatterers
Al_2O_3 powder (0.3 μm)	0.89	Sigma-Aldrich, Germany	Serves as Scatterers
Konjac root powder	1.5	Fiber, Diabetic, USA	For gel formation
Carrageenan powder	1.5	Sigma-Aldrich, Germany	For gel formation
Potassium Chloride	0.7	Sigma-Aldrich, Germany	To adjust the melting and setting temperatures of the gel.
Glycerol	9.0	Sigma-Aldrich, Germany	To mimic the acoustic properties of the tissue
Gelatin from Bovine skin	0.92	Sigma-Aldrich, Germany	To increase the strength and robustness of the TMM and to mimic the human/animal tissue

The volume of TMM in this research (7.5 liters) far out grows the amount a beaker can contain (2 liters) making it difficult to have a suitable beaker, magnetic stirrer or overhead stirrer to mix the content. Therefore, an aluminum cooking pot (12 liters capacity) and a pressing rotary stainless steel hand held mixer were used to cook the TMM and continuously mixed the content manually until it was well cooked at about 95^0C (figure 1b). The steps involved in preparing the TMM are discussed as follows:

(1). The required amount of distilled water was measured out and poured inside the cooking pot.

(2). In a fume hood, the amounts of aluminium oxides ($0.3\mu m$ and $3.0\ \mu m$) and silicon carbide were also measured out using a chemical balance.

(3). The three powders were then sift together using a domestic sieve to ensure that they mix properly. The powder mixtures were sifting inside the pot containing the distilled water and mixed thoroughly to remove any clumps that may be formed.

(4). The mixture was degassed using a vacuum pump at 4.8 Mpa (700 psi) for about 30 minutes to remove air bubbles. The process was repeated until all the air bubbles were eliminated.
(5). The entire system of mixture was then placed on an electric hot plate with an improvised water bath. The plate was switched on to start the cooking process. The content was continually mixed to avoid settling down of the powders.
(6). Conjac, carrageenan and gelatin powders as well as potassium chloride salt were measured out in a fume hood, sift together to ensure that they mix properly.
(7). When the temperature of the content was above 60^0C, the mixture of conjac, carrageenan, gelatin and potassium chloride powders was added in small amounts to avoid forming clumps. The system was continuously mixed to have a homogenous mixture. This process of mixing was done at few minutes interval after which the content was covered to reduce the evaporation of the TMM.
(8). The entire system was heated for about an hour when the temperature had reached 95^0C after which the glycerol was added accompanied by the addition of 10 cm^3 of 50% benzalkonium chloride solution to serve as an antifungal agent. It was continuously mixed for about 20 minutes after which the hot plate was switched off.
(9). When the container had cooled to about 80^0C, the TMM was poured inside the phantom box until it was 7.5 mm above the rods (figure 1c).

(a)

(b)

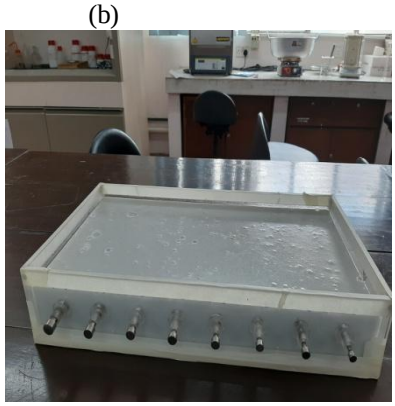

(c)

Figure 1: Procedures for preparing a vascular wall-less phantom; (a) Phantom box with horizontal rods, (b) cooking of TMM, (c) casting of the TMM inside the phantom box

This was done spontaneously not slowly so that it will distribute evenly in the mold and to ensure that it does not turn solid immediately. The Phantom box was warmed before pouring the TMM to avoid instant solidification.
(10). As the TMM finally gets cooled and settled, the rods were gradually pulled out of the phantom without rotating the rods, leaving very clean and fine lumens (holes) through the TMM. A solution of 9% glycerol was poured on top of it to prevent it from drying out on time. The multi-lumen diameter CCA phantom was then ready for ultrasound scanning.

2.3 Blood Mimicking Fluid Preparation

The BMF was prepared by a combination of 84 % w/w distilled water, 5 % w/w Propylene glycol, 11 % w/w anhydrous D(+)-Glucose as the mixture fluid with 0.8% poly (4-methylstyrene) as scatter particles. This was followed by adding 2 drops of benzalkonium chloride to serve as a preservative against bacterial manifestation. The density of the BMF was measured using a portable Density Meter (DMA 35), while the viscosity was measured using electronic rotational viscometer (Fungilab). The pumping of the BMF was actualized using a 50130 centrifugal multi-flow pump produced by the German Society for Applied Medical Physics and Technology (GAMPT), capable of delivering up to 10 liters/minute. Care was taken to ensure that the BMF was not left inside the phantom after use to avoid settling of the scatter particles. The phantom was flushed with glycerol solution to remove the BMF completely and avoid changing the composition of the TMM while it is being stored at room temperature.

2.4 Measurements of speed of sound, Attenuation and Backscatter power

The acoustic properties of the BMF and TMM (speed of sound, attenuation and backscatter) were measured by pulse echo (PE) method using the A-scan (GAMPT) technique. The backscatter power of the BMF was measured at different radio frequency signals by calculating the average power spectrum through applying the Fast Fourier Transform (FFT) generated by the A-scan GAMPT software at 5 MHz. This was done at different concentrations of the scatter particles poly (4-methylstyrene) to find out if the BMF simulates the real human blood. The backscatter coefficients were directly read on the screen of the A-mode PE technique.

2.5 Doppler Ultrasound Scanning

A digital clinical Hitachi HI Vision Avius ultrasound scanning machine connected with a linear array transducer (probe) EUP-L74M with frequencies ranging from 5 to 13 MHz was used to get image information from the multi-lumen diameter vascular wall-less flow phantom. The phantom was placed on a flat table and connected to the pump with the aid of plastic tubes to pump the BMF (figure 2).

Figure 2: Ultrasound measurements of hemodynamic parameters using the Hitachi ultrasound machine

This fluid was pumped through each lumen at a flow rate of 1500 ml/min (for both steady and pulsed flow) and B-mode images (transverse and longitudinal) of the lumen diameters in the phantom were displayed on the screen of the scanning machine. The diameters were measured three times at different points within the lumen (close to first end, at the middle and close to the second end of the lumen) with the aid of the machine's caliper after which their averages were recorded to validate their sizes. These measurements of lumen diameter were done during steady/continuous flow. Measurements of peak systolic velocity (PSV), end-diastolic velocity (EDV), mean or average velocity (V_m), pulsatility index (PI) and resistivity index were carried out by color Doppler and Pulse- wave (PW) Doppler systems during pulsatile flow. The angle of beam (insonation angle) was set at the center of the flow at 60^0 [26, 27] with the required sample volume and entrance length of 4cm across the 8 different diameters. This was to obtain maximum and correct values of the flow velocities since the values increased from the walls of the lumen until the peak is reached at the center of the lumen. To ensure laminar flows, the inlet length was obtained from the equation [28];

$$L = 0.04 \times D \times Re \quad \ldots\ldots \quad 1$$

Where Re is the Reynolds number, given by;

$$\mathrm{Re} = \frac{\rho v D}{\mu} \quad \ldots\ldots \quad 2$$

With ρ as the BMF density, v as the viscosity and D is the diameter.

III. Results

3.1. Physical and Acoustic Properties of BMF and TMM

The BMF prepared has a density of 1.04 ± 0.01 g/cm^3, viscosity of 4.30 ± 0.05 mpa.s, speed of sound of 1580.00 ± 0.30 m/s and attenuation of 0.02 ± 0.01 dB/cm at 5 MHz. These results are within the acceptable ranges for the physical and acoustic properties of a BMF by the International Electrochemical Commission (IEC) for Doppler ultrasound flow phantoms [29, 30, 31, 32, 33]. Results showed a linear dependence of backscatter power on increasing the particle concentrations of Poly (4-methystyrene) [34], while the attenuation increases linearly with increase in frequency as shown in figures 3a and 3b. The average value for the speed of sound of the TMM was found to be 1548.00 ± 0.07 m/s while the attenuation was 0.50 ± 0.02 dB/cm at 5 MHz frequency.

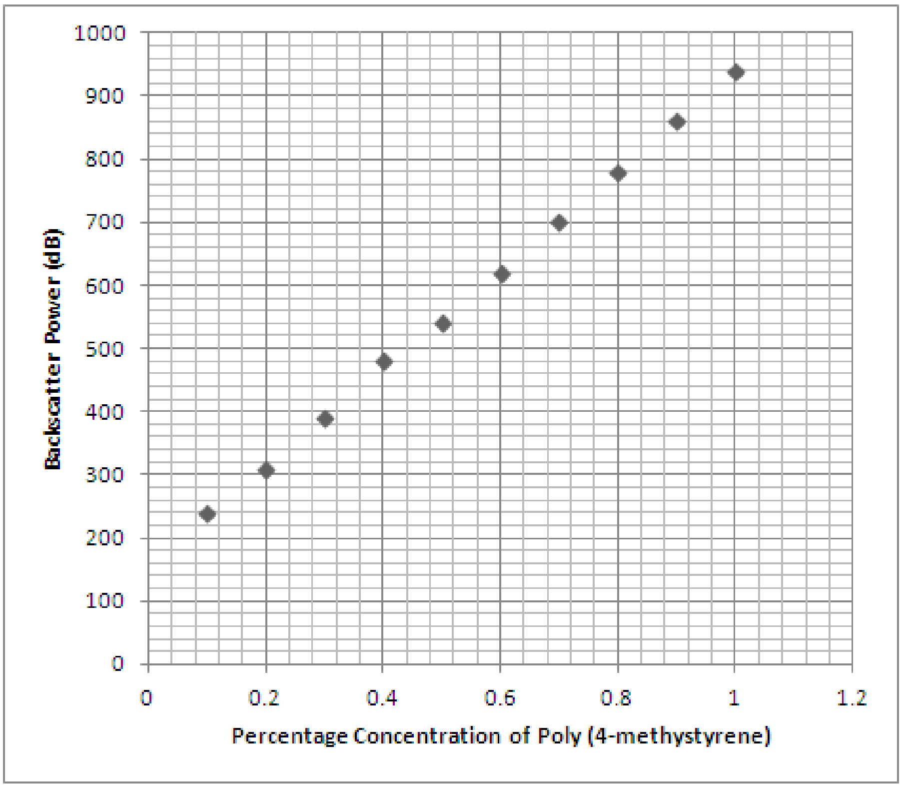

(a)

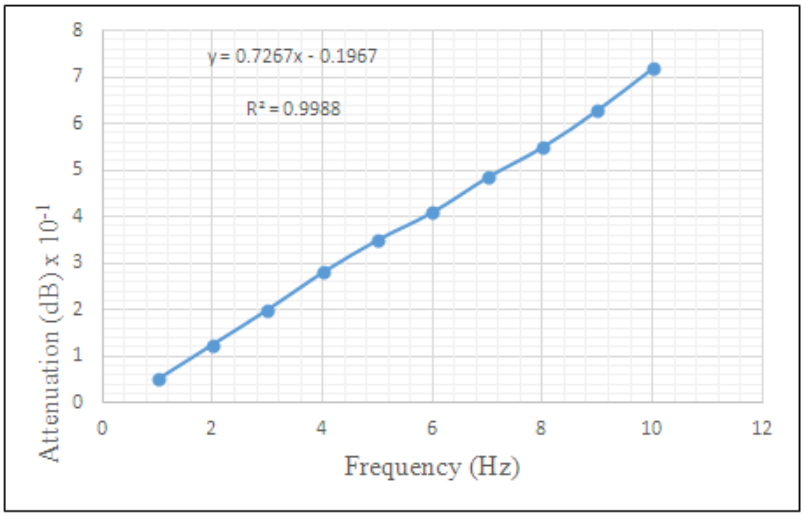

(b)

Figure 3: (a) Relative backscatter from BMF under uniform flow plotted against particle concentration for Poly (4-methylstyrene) particles of size 3-8 μm, (b) Linear graph of the attenuation at different frequencies.

3.2. Geometry of the TMM Wall-les Phantom Using B-mode Imaging

Brightness-Mode (B-Mode) gray-scale images of the transverse (figure 4) and longitudinal (figure 5) sections of the multi-lumen diameter CCA phantom revealed that the lumens were well formed with their average diameters measured during continuous flow to be the same as the original design as shown in table 2.

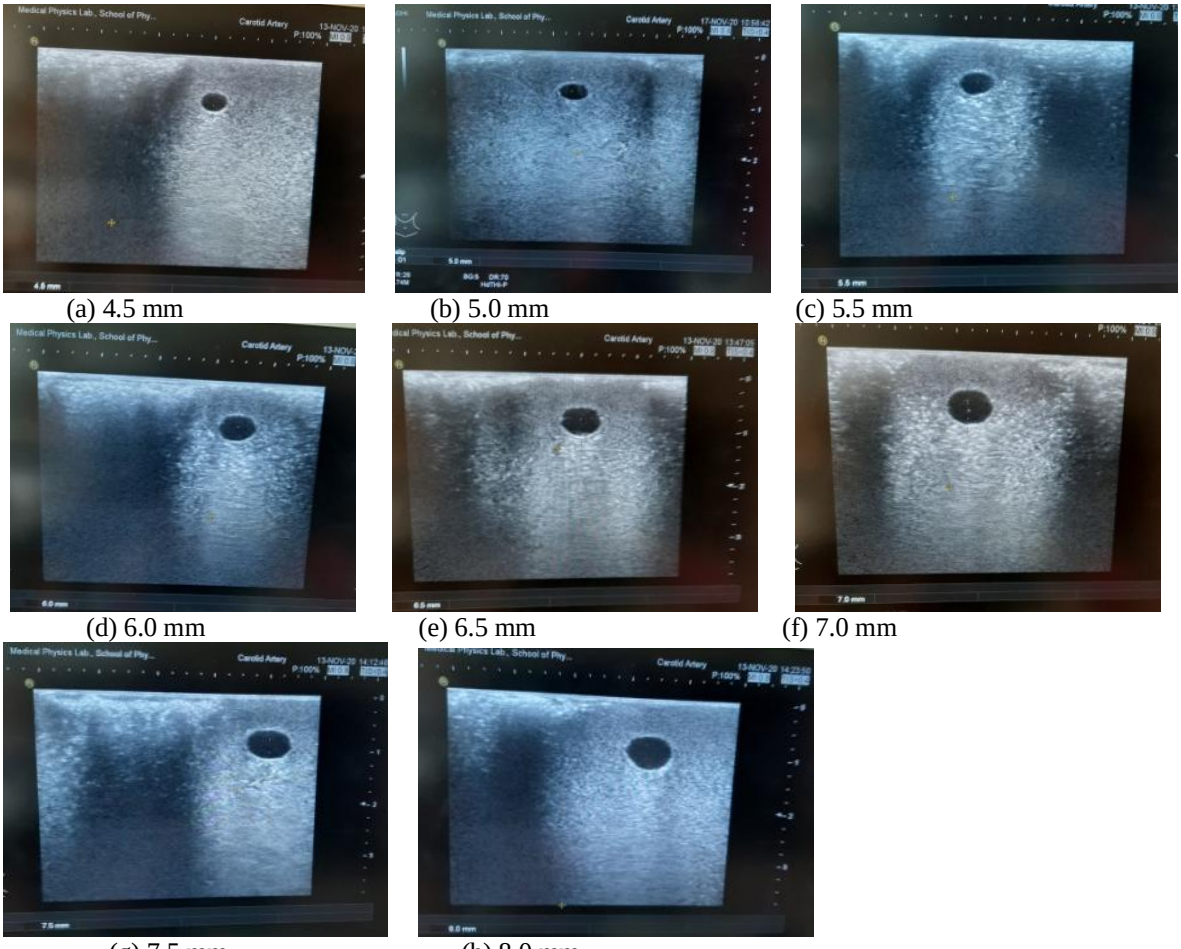

(a) 4.5 mm (b) 5.0 mm (c) 5.5 mm

(d) 6.0 mm (e) 6.5 mm (f) 7.0 mm

(g) 7.5 mm (h) 8.0 mm

Figure 4: B-Mode transverse images of the lumen diameters without the BMF

(a) 4.5 mm

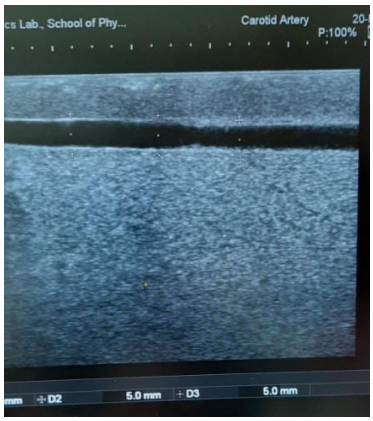

(b) 5.0 mm

(c) 5.5 mm

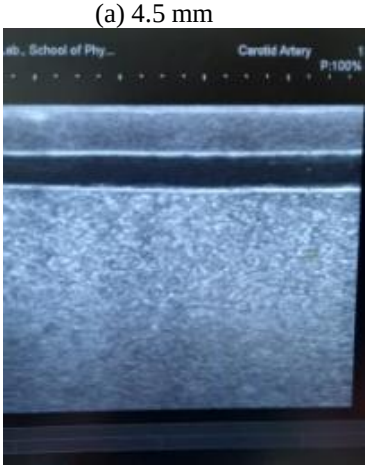

(d) 6.0 mm

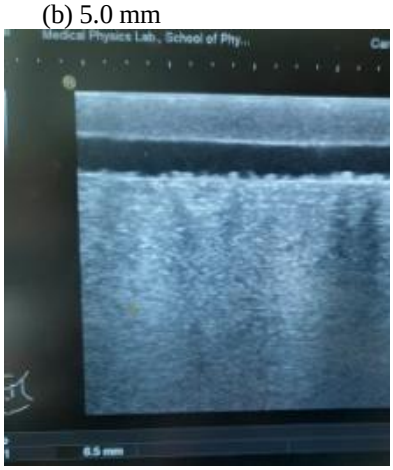

(e) 6.5 mm

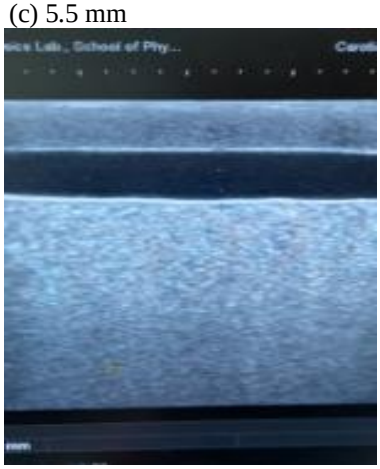

(f) 7.0 mm

(g) 7.5mm

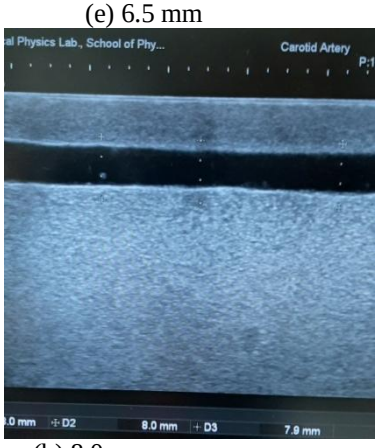

(h) 8.0 mm

Figure 5: B-Mode longitudinal images of the lumen diameters without the BMF

Table 2: Measurements of Lumen Diameters during Continuous Flow of BMF

Original Lumen Diameter (mm)	Phantom Lumen Diameter at one End (mm)	Phantom Lumen Diameter at Middle (mm)	Phantom Lumen Diameter at Second end (mm)	Average Lumen Diameter of Phantom (mm)
4.5	4.4	4.5	4.6	4.5
5.0	5.0	5.0	5.0	5.0
5.5	5.6	5.4	5.5	5.5
6.0	6.0	6.0	6.0	6.0
6.5	6.5	6.5	6.5	6.5
7.0	7.0	7.0	7.0	7.0
7.5	7.5	7.5	7.5	7.5
8.0	8.0	8.0	8.0	8.0

The image brightness (contrast resolution) for both axial (linear or longitudinal) resolution and lateral (perpendicular) resolution were seen to increase with increasing the frequency (5-13 MHz) [6]. The Pixel intensity of the TMM also increased with increasing the frequencies [35].

3.3. Colour-mode and Pulse-wave Doppler measurements of Flow Velocity

The appearance of the BMF flowing inside the lumens shows a good compatibility in the acoustic properties of both the two BMF and the TMM allowing a good B-mode (figure 6a) and colour mode (figure 6b) images of the flowing BMF. The depth of the lumen from the scanning surface is a very important factor to be considered when constructing a wall-less phantom. Activation of the pulse-wave (PW) Doppler mode on the ultrasound machine (figure 6c) automatically measured the PSV, EDV, Vm, PI and RI values with results shown in table 3.

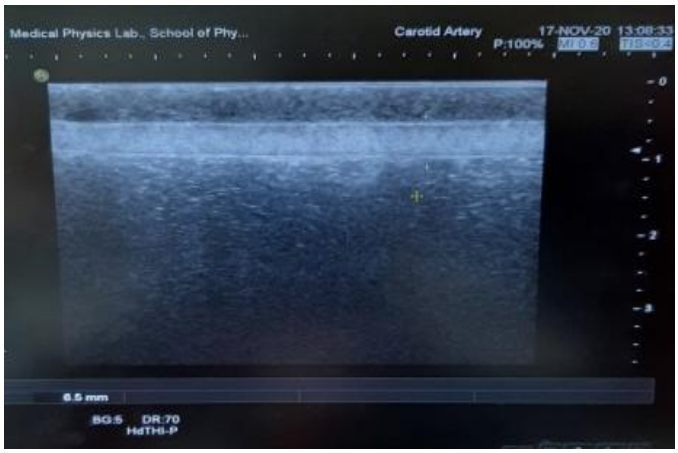

(a)

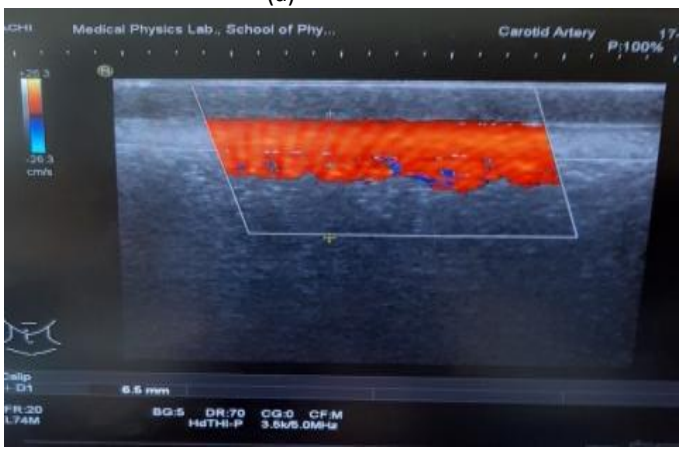

(b)

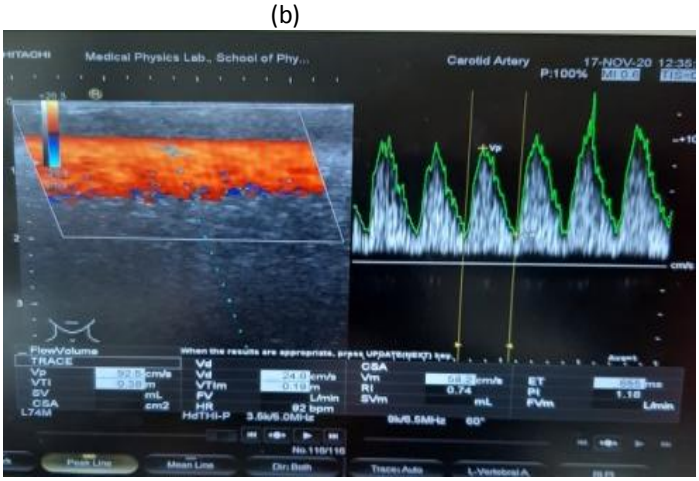

(c)

Figure 6: Color and PW modes; (a) B-mode appearance of BMF in the phantom, (b) C-mode appearance of the BMF in the phantom, (c) PW-mode for measuring the BMF flow parameters through the phantom

Table 3: Blood mimicking fluid (BMF) peak systolic velocity (PSV), end diastolic velocity (EDV), mean velocity (V_m), pulsatility index (PI) and resistivity index for different values of lumen diameters (LD)

LD (mm)	PSV (cm/s) ± 2.50	EDV(cm/s) ± 1.50	Vm (cm/s) ± 3.00	PI ± 0.10	RI ± 0.10
4.5	134.0	39.1	83.5	1.14	0.71
5.0	127.0	36.6	82.2	1.14	0.71
5.5	123.0	24.1	66.1	1.50	0.80
6.0	121.1	21.6	69.9	1.43	0.82
6.5	106.0	22.6	54.4	1.53	0.79
7.0	97.6	19.5	49.3	1.58	0.80
7.5	84.2	21.6	49.3	1.27	0.74
8.0	74.1	23.2	48.2	1.06	0.69

An analysis of the results using statistical package for social sciences (SPSS) tool showed an inverse relationship between the lumen diameter with the PSV ($P<0.01$), EDV ($p<0.05$) and Vm ($P<0.01$). Linear regression equations connecting phantom lumen diameters (LD) with PSV and EDV for BMF are given as:

$$PSV = 216.202 - 17.252LD \quad \text{.....3}$$

$$EDV = 55.665 - 4.74LD \quad \text{.....4}$$

IV. Discussion

The speed of sound of the TMM showed no much changes as the frequency was increased but a linear relationship exists between attenuation coefficients with frequency. This is because the domain of the speed of sound does not change within the same medium no matter the frequency [4]. The slide differences in some values of lumen diameter measurements found in table 2 may be as a result of some measurement errors from the operator. Continuous/steady flow was chosen over pulsatile flow for the measurement of lumen diameter because it gives the true picture of the lumen since there is no fluctuation in the flow. Apart from overcoming the problem of rupture, this phantom did not absorb water and glycerol. Therefore, the phantom can be flushed with glycerol or water to remove particles that may still be attached to the walls of the vessels after being used with the BMF. Compared to previously fabricated wall-less phantoms, this study differs in its multi-lumen diameter model but has the same chemical components and methodology of preparation with previous studies [8, 6, 2, 36]. The BMF employed for this study only differs in its ternary mixture fluid which introduced glucose as part of the fluid's component. The presence of glucose gave more accurate values of viscosity and speed of sound compared to previous BMF with higher speed of sound and viscosity [37].

The clinical application of this study is found in the fabrication and performance testing of diagnostic ultrasound phantoms which are potentially used in clinical setting especially for quality testing purposes and for training of operators in the field of ultrasound. The samples prepared can be potentially used as phantom for diagnostic ultrasonography purposes and for research training. This wall-less phantom has the advantage of avoiding mismatch problems in acoustic properties [7, 8] over walled phantoms.

The PI and RI values did not have any significant relationship with the lumen diameter, however, their values as well as the velocity values were within the acceptable range (PSV< 135 cm/s, EDV< 45 cm/s, PI from 1.5 to 2.0 and RI from 0.5 to 0.9) [38, 39, 40, 37]. By equations 3 and 4, it means that the PSV and EDV of the BMF increased with reduction or narrowing of the phantom diameter. The average velocities of the samples also increased as the lumen diameter decreases. In-vivo research has found out that cardiovascular disease such as atherosclerosis is associated with large lumen diameter and IMT in elderly people, smokers and hypertensive patients [41, 42, 43]. A slight increase in lumen diameter in diabetic and hypertensive young and old patients, while a significant increase in IMT, EDV and RI were reported by [44, 45]. Very few in-vitro researches have been reported on variations between lumen diameter and hemodynamic indices in the CCA. Results of this research can be used to do more studies on blood flow in the CCA.

The limitation of this research was the large volume of the TMM involved. Because of this large volume, there was no suitable container and means of stirring the TMM mixture. Even though we improvised a water bathe for steady distribution of heat, it was a difficult task to mix the content because it was manually done with a rotary hand mixer leading to having some debris in the TMM. It was not possible to completely eliminate air bubbles during the manual mixing. Evaporation of the TMM was also a challenge that could not be avoided, this made the attenuation of the TMM phantom to be a little higher than the required standard. More research needs to be conducted on wall-less phantoms with smaller thicknesses of 1 mm to 2 mm to test the robustness of the Konjac- carrageenan and gelatin based phantoms to mimic the arteries of Rats.

V. Conclusion

We have described the design of a robust multi-lumen diameter common carotid artery wall-less phantom with a thickness (scanning depth) of 7.5 mm that was useful in studying velocity of BMF. This value of thickness is an improvement on the previous phantom of thickness 15 mm by [36]. Even at this smaller thickness (7.5 mm), the phantom was robust and strong without any rupture at flows up to 1500 ml/min. The phantom showed very good physical and acoustic properties, B-mode images, C-mode and PW-mode formations. The lumen diameter was found to be inversely related with the PSV, EDV and V_m which gave useful information on assessing the degree of stenosis in the CCA.

Conflicts of interest

There are no conflicts of interest.

Financial support and sponsorship

There is no funding for this research

Acknowledgement

We acknowledge the contributions of Prof. Mohammed Zubir who initiated the research, provided support (under the grant number 1001/PFIZIK/822173) and supervisory role. Dr. Nursakinah Suardi gave technical advice, support (under the grant number 1001/PFIZIK/822173) and editing of the manuscript. Dr. Dakok Kyense performed the experiment and contributed in drafting of the manuscript. Dr. Ammar Oglat and Mr Nabasu Seth contributed with essential materials needed for the manuscript drafting and also participated in prove reading the manuscript. All authors read and approved the final manuscript.

References

[1]. Homagni S. R., Guoqing Z., Zhengchun L., Hanping W., Tianyi M. K., Haitao R., Pan L., et al. (2012). Direct and Doppler angle-independent measurement of blood flow velocity in small-diameter vessels using ultrasound microbubbles. *Clinical Imaging*, **36:** 577–583. https://doi.org/10.1016/j.clinimag.2012.01.026

[2]. Kenwright, D. A., Laverick, N., Anderson, T., Moran, C. M., Hoskins, P. R. (2015). Wall-less flow phantom for high-frequency ultrasound applications. In *Ultrasound in Medicine and Biology*. **41**(3): 890–897. https://doi.org/10.1016/j.ultrasmedbio.2014.09.018

[3]. Kenwright, D. A., Sadhoo, N., Rajagopal, S., Anderson, T., Moran, C. M., Hadoke, P. W., et al. . (2014). Acoustic Assessment of a Konjac-Carrageenan Tissue-Mimicking Material at 5-60MHz. In *Ultrasound in Medicine and Biology*. **40**(12): 2895–2902. https://doi.org/10.1016/j.ultrasmedbio.2014.07.006

[4]. Sun C., Stephen D. P., Jacinta E. B., Anna J., Bill E., Mairead B. B., Vassilis S., et al. (2012). The Speed of Sound and Attenuation of an IEC Agar-Based Tissue-Mimicking Material for High Frequency Ultrasound Applications. *Ultrasound in Med & Biol*, **38**(7): 1262–1270. https://doi.org/10.1016/j.ultrasmedbio.2012.02.030

[5]. Zhou, X., Kenwright, D. A., Wang, S., Hossack, J. A., Hoskins, P. R. (2017). Fabrication of two flow phantoms for doppler ultrasound imaging. *IEEE Transactions on Ultrasonics, Ferroelectrics, and Frequency Control*, **64**(1): 53–65.

[6]. Ramnarine, K. U. V. R., Nderson, T. O. M. A., Hoskins, P. R. H. (2001). Construction and Geometric Stability of Physiological Flow Rate Wall-Less Stenosis Phantoms. *Ultrasound in Medicine & Biology*, **27**(2): 245–250.

[7]. Guo Z., Fenser A. (1996). Three-Dimensional Power Doppler Imaging: A Phantom Study to Quantify Vessel Stenosis. *Ultrasound in Med. & Biol.*, **22**(8): 1059–1069.

[8]. Rickey, D. W., Picot, P. A., Christopher, D. A., Fenster, A. (1995). A wall-less vessel phantom for Doppler ultrasound studies. *Ultrasound in Medicine and Biology*. **21**(9): 1163–1176. https://doi.org/10.1016/0301-5629(95)00044-5

[9]. Meagher, S., Poepping, T. L., Ramnarine, K. V., Black, R. A., Hoskins, P. R. (2007). Anatomical flow phantoms of the nonplanar carotid bifurcation, Part II: Experimental validation with Doppler ultrasound. *Ultrasound in Medicine and Biology*. **33**(2): 303–310. https://doi.org/10.1016/j.ultrasmedbio.2006.08.004

[10]. Grant, E. G., Benson, C. B., Moneta, G. L., Alexandrov, A. V, Baker, J. D., Bluth, E. I., et al. (2003). Carotid Artery Stenosis : Gray-Scale and Doppler US Diagnosis — Society of Radiologists in Ultrasound Consensus Conference 1. *Society of Radiologists in Ultrasound Consensus Conference*, **229:** 340–346.

[11]. Shivani G., Shivali V. K., Suresh P. (2016). *Colour Doppler Evaluation of Extracranial Carotid Arteries_ A Clinical and Radiological Correlation*. **10**(1): 6-10. https://doi.org/10.7860/JCDR/2016/15426.7130

[12]. Samrin H., Manoj M., Jasvir S., Navkiran K., Raminderpal S. S., Rajesh B. (2017). *Colour Doppler Evaluation of Extracranial Carotid Artery in Patients Presenting with Acute Ischemic Stroke and Correlation with Various Risk Factors*. **11**(3): 1-5. https://doi.org/10.7860/JCDR/2017/25493.9541

[13]. Lai, S. S. M., Yiu, B. Y. S., Poon, A. K. K., Yu, A. C. H. (2013). Design of anthropomorphic flow phantoms based on rapid prototyping of compliant vessel geometries. *Ultrasound in Medicine and Biology*. **39**(9): 1654–1664. https://doi.org/10.1016/j.ultrasmedbio.2013.03.015

[14]. Galluzzo, F., Leonardo, F., Ceruti, A., De Marchi, L., Corsi, C. (2015). Design of anthropomorphic atherosclerotic carotid artery flow phantoms for ultrasound images. *Computing in Cardiology*, **42**: 721–724. https://doi.org/10.1109/CIC.2015.7411012

[15]. Adrian J. Y. C., Chung K. H., Billy Y. S. Y., Alfred C. H. (2016). Walled Carotid Bifurcation Phantoms for Imaging Investigations of Vessel Wall Motion and Blood Flow Dynamics. *IEEE Transactions on Ultrasonics, Ferroelectrics, and Frequency Control.* **63**(11): 1852-1864.

[16]. Onaizah, O., Poepping, T. L., Zamir, M. (2017). A model of blood supply to the brain via the carotid arteries: Effects of obstructive vs. sclerotic changes. In *Medical Engineering and Physics*. **49:** 121–130. https://doi.org/10.1016/j.medengphy.2017.08.009

[17]. Filippou, V., Tsoumpas, C. (2018). Recent advances on the development of phantoms using 3D printing for imaging with CT, MRI, PET, SPECT, and ultrasound. In *Medical Physics*. **45**(9): 740–760. https://doi.org/10.1002/mp.13058

[18]. Chee, A. J. Y., Yiu, B. Y. S., Ho, C. K.,Yu, A. C. H. (2018). Arterial Phantoms with Regional Variations in Wall Stiffness and Thickness. *Ultrasound in Medicine and Biology*, **44**(4): 872–883. https://doi.org/10.1016/j.ultrasmedbio.2017.12.008

[19]. Chayer, B., Van Den Hoven, M., Cardinal, M. H. R., Li, H., Swillens, A., Lopata, R., Cloutier, G. (2019). Atherosclerotic carotid bifurcation phantoms with stenotic soft inclusions for ultrasound flow and vessel wall elastography imaging. *Physics in Medicine and Biology*, **64**(9): 1–12. https://doi.org/10.1088/1361-6560/ab1145

[20]. Elvira, L., Durán, C., Higuti, R. T., Tiago, M. M., Ibáñez, A., Parrilla, M., Valverde, E., Jiménez, J., Bassat, Q. (2019). Development and Characterization of Medical Phantoms for Ultrasound Imaging Based on Customizable and Mouldable Polyvinyl Alcohol Cryogel–Based Materials and 3-D Printing: Application to High-Frequency Cranial Ultrasonography in Infants. In *Ultrasound in Medicine and Biology*. **45**(8): 2226–2241. https://doi.org/10.1016/j.ultrasmedbio.2019.04.030

[21]. Krejza, J., Arkuszewski, M., Kasner, S. E., Weigele, J., Ustymowicz, A., Hurst, R. W., et al. (2006a). Carotid artery diameter in men and women and the relation to body and neck size. In *Stroke*. **37(**4):. 1103–1105. https://doi.org/10.1161/01.STR.0000206440.48756.f7

[22]. Limbu, Y. R., Gurung, G., Malla, R., Rajbhandari, R., Regmi, S. R. (2006). Assessment of carotid artery dimensions by ultrasound in non-smoker healthy adults of both sexes. In *Nepal Medical College journal : NMCJ* .**8**(3): 200–203).

[23]. Krejza, J., Arkuszewski, M., Kasner, S. E., Weigele, J., Ustymowicz, A., Hurst, R. W., et al. (2006b). Carotid Artery Diameter in Men and Women and the Relation to Body and Neck Size. https://doi.org/10.1161/01.STR.0000206440.48756.f7

[24]. Tuncer, I. (2018). Angiographic morphometry of internal carotid , external carotid and common carotid artery in Turkish adult. *International Journal of Medical and Health Research*, **4**(12): 132–135.

[25]. Ammar A. O., Matjafri M. Z., Suardi N., Oglat M. A., Abdelrahman M. A., et al. (2018b). Chemical items used for preparing tissue-mimicking material of wall-less flow phantom for Doppler ultrasound imaging. In *Journal of Medical Ultrasound*. **26**(3): 123–127. https://doi.org/10.4103/JMU.JMU

[26]. Roman, M. J., Naqvi, T. Z., Gardin, J. M., Gerhard-Herman, M., Jaff, M., Mohler, E. (2006). Clinical application of noninvasive vascular ultrasound in cardiovascular risk stratification: A report from the American Society of Echocardiography and the Society for Vascular Medicine and Biology. *Vascular Medicine*, **11**(3): 201–211. https://doi.org/10.1177/1358863x06070511

[27]. Lee, W. (2013). General principles of carotid Doppler ultrasonography. *Ultrasonography*. **33**(1): 11–17. https://doi.org/10.14366/usg.13018

[28]. Nichols W. W., Michael F. O., Charalambos V., Arnold P. H. (2011). *McDonald's Blood Flow in Arteries Theoretical, Experimental and Clinical Principles* (6th ed.). CRC Press.

[29]. Ramnarine, K. V., Nassiri, D. K., Hoskins, P. R., Lubbers, J. (1998). Validation of a new blood-mimicking fluid for use in Doppler flow test objects. In *Ultrasound in Medicine and Biology*. **24(**3): 451–459. https://doi.org/10.1016/S0301-5629(97)00277-9

[30]. Browne, J. E., Ramnarine, K. V., Watson, A. J., Hoskins, P. R. (2003). Assessment of the acoustic properties of common tissue-mimicking test phantoms. In *Ultrasound in Medicine and Biology*. **29**(7): 1053–1060. https://doi.org/10.1016/S0301-5629(03)00053-X

[31]. Samavat H., Evans J. A. (2006). An ideal blood mimicking fluid for doppler ultrasound phantoms. *Journal of Medical Physics*. **31**(4): 275–278.

[32]. Yoshida A. K. T, Tomoji S., Kazuishi K., Toshio Y. K. (2012). Blood-Mimicking Fluid for Testing Ultrasonic Diagnostic Instrument Blood-Mimicking Fluid for Testing Ultrasonic Diagnostic Instrument. *Japanese Journal of Applied Physics*, **51**(7). https://doi.org/10.1143/JJAP.51.07GF18

[33]. Yoshida, T., Sato, K., Kondo, T. (2014). Blood-mimicking fluid using glycols aqueous solution and their physical properties. *Japanese Journal of Applied Physics*, **53**(75): 8–13. https://doi.org/http://dx.doi.org/10.7567/JJAP.53.07KF0

[34]. Oglat, A. A., Matjafri, M. Z., Suardi, N., Abdelrahman, M. A., Oqlat, M. A., Oqlat, A. A. (2018a). A new scatter particle and mixture fluid for preparing blood mimicking fluid for wall-less flow phantom. In *Journal of Medical Ultrasound*. **26(**3): 134–142. https://doi.org/10.4103/JMU.JMU_7_18

[35]. Pazinato, D. V, Stein, B. V, Almeida, W. R. De, Werneck, R. D. O., Pedro R. M. (2014). Pixel-Level Tissue Classification for Ultrasound Images. *IEEE Journal of Biomedical and Health Informatic*. 1–13. https://doi.org/10.1109/JBHI.2014.2386796

[36]. Ammar, A. O., Matjafri, M., Suardi, N., Oqlat, M. A., Oqlat, A. A., Abdelrahman, M. A., et al. (2018a). Characterization and Construction of a Robust and Elastic Wall-Less Flow Phantom for High Pressure Flow Rate Using Doppler Ultrasound Applications. *Natural and Engineering Sciences*. **3**(3): 359–377. https://doi.org/10.28978/nesciences.468972

[37]. Oglat, A. A., Matjafri, M. Z., Suardi, N., Oqlat, M. A., Abdelrahman, M. A., Oqlat, A. A. (2018b). A review of medical doppler ultrasonography of blood flow in general and especially in common carotid artery. In *Journal of Medical Ultrasound*. **26(**1): 3–13. https://doi.org/10.4103/JMU.JMU_11_17

[38]. Govind B. C., Dimitri A. P., Andrea M., Oscar M. N. (2008). Normal Doppler Spectral Waveforms of Major Pediatric Vessels: Specific Patterns. *Radiographics*, **28**(3): 691–707. https://doi.org/10.1148/rg.283075095

[39]. Gerhard-herman, M., Gardin, J. M., Jaff, M., Mohler, E., Roman, M. (2006). Guidelines for noninvasive vascular laboratory testing : a report from the American Society of Echocardiography and the Society for Vascular Medicine and Biology. *Vascular Medicine*, **11**(3): 183–200. https://doi.org/10.1177/1358863x06070516

[40]. Slovut, D. P., Javier M. R., Kathleen M. H., James D., Michael R. J. (2010). Detection of common carotid artery stenosis usingduplex ultrasonography: A validation study with computed tomographic angiography. *Journal of Vascular Surgery*, **51**(1): 65–70.

[41]. Sedaghat, S., van Sloten, T. T., Laurent, S., London, G. M., Pannier, B., Kavousi, M., et al. (2018). Common Carotid Artery Diameter and Risk of Cardiovascular Events and Mortality. In *Hypertension*. **72(**1): 85–92). https://doi.org/10.1161/hypertensionaha.118.11253

[42]. Chyi-Huey B., Jiunn-Rong C., Hou-Chang C., Wen H. P. (2007). Lower blood flow velocity, higher resistance index, and larger diameter of extracranial carotid arteries are associated with ischemic stroke independently of carotid atherosclerosis and cardiovascular risk factors. *Journal of Clinical Ultrasound*. **35**: 322–330. https://doi.org/10.1002/jcu.20351

[43]. Toshifumi M., Shunroku B., Jun O. (2000). Potential of Carotid Enlargement as a Useful Indicator Affected by High Blood Pressure in a Large General Population of a Japanese City. *Stroke*, **31**(12): 2958–2965. https://doi.org/https://doi.org/10.1161/01.STR.31.12.2958

[44]. Al-sabbagh, A. A., Essa, S. I., Saleh, A. Z. (2020). Resistive index is an early indicator for flow deterioration in comparison with intima media thickness for patients with hypertension and diabetes in relation to age. *J Cardiovasc Disease Res*, **11**(1), 16–19. https://doi.org/10.5530/jcdr.2020.11.05

[45]. Mehravar R., Elham H., Hassan M., Mohammadreza S. (2017). Appraisal of different ultrasonography indices in patients with carotid artery atherosclerosis. *EXCLI Journal*, **16**: 727–741.